ACS APPLIED MATERIALS & INTERFACES

Research Article

www.acsami.org

Investigation of a Branchlike MoO_3/Polypyrrole Hybrid with Enhanced Electrochemical Performance Used as an Electrode in Supercapacitors

Xia Zhang,[†,‡] Xianzhong Zeng,[†,‡] Min Yang,[†] and Yanxing Qi*[,†]

[†]State Key Laboratory for Oxo Synthesis and Selective Oxidation, Lanzhou Institute of Chemical Physics, Chinese Academy of Sciences, Lanzhou 730000, China

[‡]Graduate University of Chinese Academy of Sciences, Beijing 100049, China

ABSTRACT: A branchlike MoO_3/polypyrrole conductive nanocomposite was facilely prepared by wrapping a homogeneous polypyrrole (PPy) layer around MoO_3 nanobelts via the in situ oxidative polymerization of a self-assembled pyrrole monomer. X-ray powder diffraction characterization demonstrated that the PPy polymer does not hinder the crystallization of the MoO_3 nanobelts substrate. The electrochemical tests show that the specific capacitance of 129 F g^{-1} for the MoO_3/PPy hybrid is higher than both pristine MoO_3 and pure PPy. Moreover, the hybrid electrode with good electrical conductivity displays good cyclic stability of 90% retention after 200 cycles of charge/discharge. These results indicate a promising potential application of the MoO_3/PPy nanocomposite for use as an effective electrode material in supercapacitors.

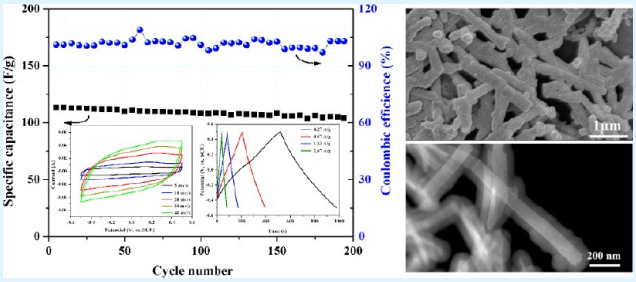

KEYWORDS: *molybdenum trioxide, polypyrrole, hybrid, energy storage, supercapacitor*

1. INTRODUCTION

Electrochemical capacitors, also called supercapacitors, are one of the most promising electrochemical energy-storage systems and have attracted more attention than dielectric capacitors and batteries because of their high energy density and long cycle stability,[1−3] which play an increasingly important role in power-source applications such as hybrid electric vehicles, short-term power sources for mobile electronic devices, and so forth.[4] Generally, according to the charge/discharge mechanism, supercapacitors can be classified into two categories: electrical double-layer capacitors (EDLCs), which commonly use carbon-active materials, and pseudocapacitors, which use redox-active transition-metal-oxide materials. Ruthenium oxide (RuO_2) is widely recognized as the best electrode material because of its high specific capacitance.[5,6] However, it is expensive, which limits its extensive application, and other low-cost transition-metal oxides such as MnO_2, MoO_x, CoO_x, NiO_x, and Fe_2O_3 have been developed as alternatives.[7−11] Among these candidates, molybdenum trioxide (MoO_3), which has been extensively investigated as an electrode material in lithium-ion batteries,[12] has also attracted considerable interest as a promising supercapacitive material because of its low cost, nontoxicity, high electrochemical activity, and more environmentally benign nature than other transition-metal oxides.[13−19] Nevertheless, the commercial recognition of MoO_3 material has been hindered because of its poor inherent electrical conductivity, which results in a low power density, narrow operation voltage window, and sluggish faradaic redox kinetics. To enhance its electrical conductivity and the subsequent high capacitance and good cycling stability, positive attempts have been made to improve the electrochemical performance of MoO_3-based electrodes by introducing some effective materials.[20−22] For example, the deposition of the MoO_3 nanodots on multiwalled carbon nanotubes can enhance its electrochemical performance.[20]

Polypyrrole (PPy) is an interesting conductive polymer that shows more advantages because of its high electrical conductivity, easy synthetic procedure, enhanced thermal and chemical stability, environmental friendliness, and low cost.[23−25] However, the poor processability and cycling stability as well as the inferior mechanical property, which may be due to the collapse of the polymer backbone during a limited number of charge/discharge cycles, have limited the applications of PPy.[26] Therefore, it is often hybridized with other suitable supports, such as carbon nanotubes, graphene oxide, inorganic transition-metal oxides, and so forth , to prepare a composite and is used in supercapacitors with better cyclability, specific capacitance, and mechanical stability.[25,27−29] Furthermore, it is well-known that the hybridization of PPy with different types of capacitive materials is attractive because it enables the formation of hybrid compounds with versatile and tunable properties that are superior to the individual

Received: October 25, 2013
Accepted: December 24, 2013
Published: December 24, 2013

materials. Recently, this research subject has become a hotspot in the supercapacitor field. Therefore, developing a PPy-based composite could facilitate its potential application as an electrode material for high-performance supercapacitors in the future. To the best of our knowledge, although MoO_3 has been used as an energy-storage material because of its unique structural anisotropy, the synthesis and application of a MoO_3/PPy hybrid for use as an electrode material in supercapacitors has been rarely reported. Recently, Liu and co-workers reported polypyrrole-coated α-MoO_3 nanobelts (prepared by hydrothermal method) used as the anode material in a 0.5 M K_2SO_4 aqueous electrolyte. However, the electrochemical tests showed that the specific capacity was just about 50 F g^{-1} for the PPy@MoO_3 nanocomposite, which may be due to its high charge-transfer resistance (R_{ct} = 81.02 Ω).[30]

Herein, we report a MoO_3/PPy hybrid that was successfully fabricated by homogeneous coating of a PPy layer around MoO_3 nanobelts via the in situ oxidative polymerization of a pyrrole monomer in aqueous solution. In the course of synthesizing MoO_3 nanobelts via a sonochemical procedure, a trace amount of poly(ethylene glycol) (PEG) was added into the molybdenum precursor solution to be employed as a metal-colloids stabilizer to prevent their agglomeration and precipitation via the binding of metal ions to pseudocrown ether cavities formed by PEG. Importantly, electrochemical tests indicate that the MoO_3/PPy nanocomposite, with a low internal resistance and charge-transfer resistance (R_{ct} = 2.36 Ω), exhibits a high capacitance and excellent cycling stability as an electrode material for supercapacitors in 1 M Na_2SO_4 electrolyte, which makes it a promising candidate for the fabrication of electrochemical energy-storage devices.

2. EXPERIMENTAL SECTION

2.1. Material Synthesis. The MoO_3 nanobelts were prepared via a sonochemical process. In a typical procedure, 2.2 M HNO_3 was dropped into 30 mL of 0.1 M Na_2MoO_4 solution to adjust the pH to around 1.5, and then 20 mg of PEG (dissolved in 40 mL of deionized water) was slowly added. After stirring for 10 min, the obtained mixed solution was irradiated by ultrasound for 4 h. The resulting precipitate was centrifuged and washed successively with deionized water and ethanol and then dried at 60 °C under vacuum to obtain the MoO_3 nanobelts.

The MoO_3/PPy nanocomposite was synthesized by in situ oxidative polymerization. A typical synthesis was as follows. Freshly prepared MoO_3 (0.1 g) nanobelts were fully dispersed in 20 mL of deionized water at ambient temperature and then transferred into an ice bath (cooled to below 5 °C). To this vigorously stirred suspension was added 0.2 mL of pyrrole, and stirring was continued for 0.5 h. Then, 0.4 g of $(NH_4)_2S_2O_8$ (dissolved in 10 mL of deionized water) was slowly dropped into the above solution, and the polymerization was performed overnight in an ice bath. The black-colored solution was centrifuged and then dried at 60 °C for 12 h under vacuum to obtain the MoO_3/PPy nanocomposite.

2.2. Material Characterization. The obtained MoO_3 nanobelts and MoO_3/PPy hybrid were characterized by X-ray powder diffraction (XRD) on a Rigaku D/Max-3B diffractometer with Cu Kα radiation (λ=1.54 Å). The microstructure was studied by transmission electron microscopy (TEM, JEM JEOL 2100) and field-emission scanning electron microscopy (FESEM, JSM-6701F). The qualitative information was obtained by Fourier transform infrared spectroscopy (FTIR, Thermo Nicolet 5700).

2.3. Electrochemical Measurements. A typical three-electrode test cell was used for electrochemical measurements on a CHI660D (Chenhua, Shanghai, China) electrochemical working station. All of the measurements were carried out in a 1 M Na_2SO_4 aqueous electrolyte solution at room temperature. The working electrode was fabricated by mixing the electroactive material, carbon black and poly(tetrafluoroethylene) at a weight ratio of 85:10:5 to form a homogeneous slurry (the total mass of the electrode material was 9 mg). The resulting slurry was coated onto the nickel foam current collector using a blade. Then, the electrode was dried at 80 °C for 12 h. A platinum sheet and saturated calomel electrode (SCE) were used as the counter and reference electrodes, respectively. Cyclic voltammograms were recorded at different scan rates from 5 to 40 mV s^{-1} within the potential window from −0.5 to 0.5 V. Galvanostatic charge−discharge curves were performed at different current densities within the potential range from −0.5 to 0.5 V. Electrochemical impedance spectroscopy (EIS) measurements were carried out in the frequency range of 10^5 to 10^{-2} Hz.

3. RESULTS AND DISCUSSION

The X-ray powder diffraction patterns of the MoO_3 nanobelts and MoO_3/PPy nanocomposite are shown in Figure 1. The

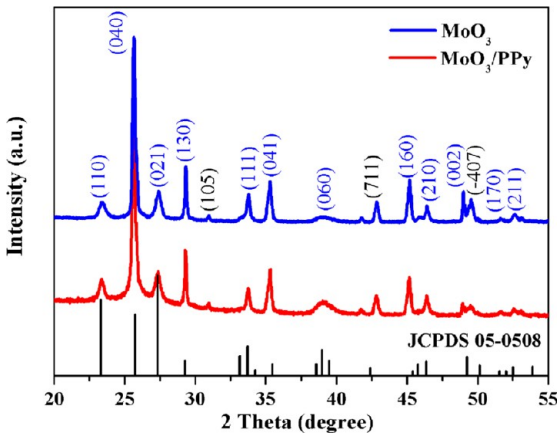

Figure 1. XRD patterns of the MoO_3 nanobelts and MoO_3/PPy nanocomposite.

sharp diffraction peaks suggest a good crystallization of the two electrode materials. For the pristine MoO_3, most of the identified peaks can be indexed to the orthorhombic α-MoO_3 (JCPDS card no. 05-0508, a = 3.962 Å, b = 13.858 Å, c = 3.697 Å) except that the diffraction peaks at 2θ = 30.9°, 42.8°, and 49.5° can be assigned to the (105), (711), and (−407) planes of molybdenum trioxide dihydrate ($MoO_3{\cdot}2H_2O$), revealing the presence of the crystallization water in the as-prepared sample. For the MoO_3/PPy nanocomposite, it has a similar XRD pattern to the pristine MoO_3, confirming the presence of MoO_3 nanobelts in the composite. At the same time, this also indicates that the PPy sheath does not hinder the crystalline behavior of the pristine MoO_3. Otherwise, as one of the main diffraction peaks, the peak width of the (060) plane is broad both in the pristine MoO_3 and MoO_3/PPy nanocomposite (compared with the virginal MoO_3 from JCPDS card 05-0508), which is likely because of the following reasons: (1) there are some crystal defects in the electrode materials, which lead to an imperfect crystal structure, and (2) the lattice distortion may occur during the crystallization of orthorhombic MoO_3 along the (060) plane.[31,32]

The FTIR spectra of the MoO_3 nanobelts and MoO_3/PPy nanocomposite are measured in the range of 4000−400 cm^{-1}. For a comparison, the FTIR spectrum of pure PPy was also obtained. In Figure 2, the FTIR spectrum of pristine MoO_3 nanobelts exhibits three typical peaks at 973, 893, and 556 cm^{-1}, which agree well with those in the literature.[33,34] The broad band at 3504 cm^{-1} corresponds to the O−H stretching

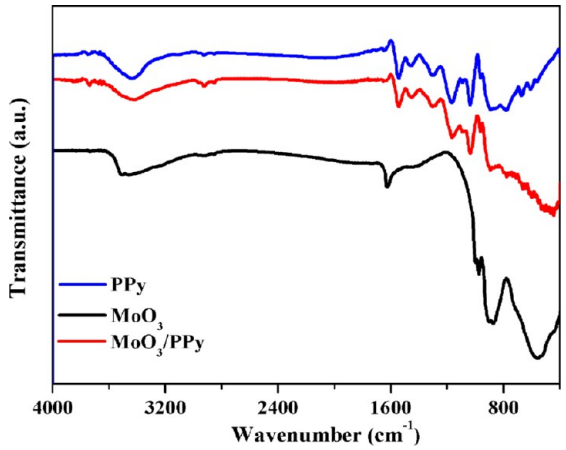

Figure 2. FTIR spectra of the MoO_3 nanobelts, pure PPy, and MoO_3/PPy nanocomposite.

vibration, whereas the peak at 1624 cm^{-1} can be attributed to the vibration of water molecules, which may be due to the absorption of moisture on the material surface. For the spectra of pure PPy and the MoO_3/PPy nanocomposite, the characteristic peaks of PPy appear. For example, the peaks at 1543 and 1454 cm^{-1} are assigned to the C=C and C−N stretching vibration in the pyrrole ring, respectively, and the bands at 1298 and 1159 cm^{-1} are attributed to the C−H in-plane ring-bending modes and the C−N in-plane ring-deformation and -bending modes, respectively.[35−37] The peaks at 1039 and 885 cm^{-1} are attributed to C−H deformation vibrations and C−H out-of-plane vibrations, respectively. Otherwise, in the spectrum of the MoO_3/PPy nanocomposite, the peak at 556 cm^{-1} is related to the bending vibration of the Mo−O−Mo shifts to 506 cm^{-1} and displays attenuation in its intensity, reflecting a mutual interaction between PPy and MoO_3.[38] With the exception of the peak at 506 cm^{-1}, the characteristic peaks for the MoO_3/PPy nanocomposite are similar to those for pure PPy, confirming the presence of PPy in the composite.

FESEM and TEM micrographs vividly depict the morphology of the prepared MoO_3 nanobelts and MoO_3/PPy nanocomposite, shown in Figure 3. From Figure 3a,b, it is obvious that the prepared MoO_3 presents 1D nanobelts with widths of 50−150 nm and lengths of 0.3−1.0 μm. As shown in Figure 3c, the branchlike MoO_3/PPy nanocomposite is 1−3 μm in length and 200−300 nm in width. In Figure 3d, it can be seen that the MoO_3 nanobelts are homogeneously wrapped by PPy to form a sealed skin and the thickness of PPy coating is about 60−100 nm.

Electrochemical measurements were performed with a three-electrode system in 1 M Na_2SO_4 electrolyte to evaluate the electrochemical performance of the MoO_3/PPy nanocomposite. For a comparison, the pristine MoO_3 nanobelts and pure PPy were also intensively studied. The cyclic voltammetry (CV) curves for the MoO_3 nanobelts, pure PPy, and MoO_3/PPy nanocomposite are presented in Figure 4a at a scan rate of 10 mV s^{-1}. Obviously, a remarkable difference can be observed in the CV loop area among these three electrodes, and the increased current of the CV curve for the MoO_3/PPy nanocomposite clearly demonstrates that the electrochemical behavior of this hybrid is distinctly improved after coating the MoO_3 nanobelts with PPy via in situ oxidative polymerization. To research the properties of the MoO_3/PPy nanocomposite electrode further, CV curves at various scan rates were collected. From Figure 4b, all of the CV curves exhibit an approximately rectangular shape without any obvious redox

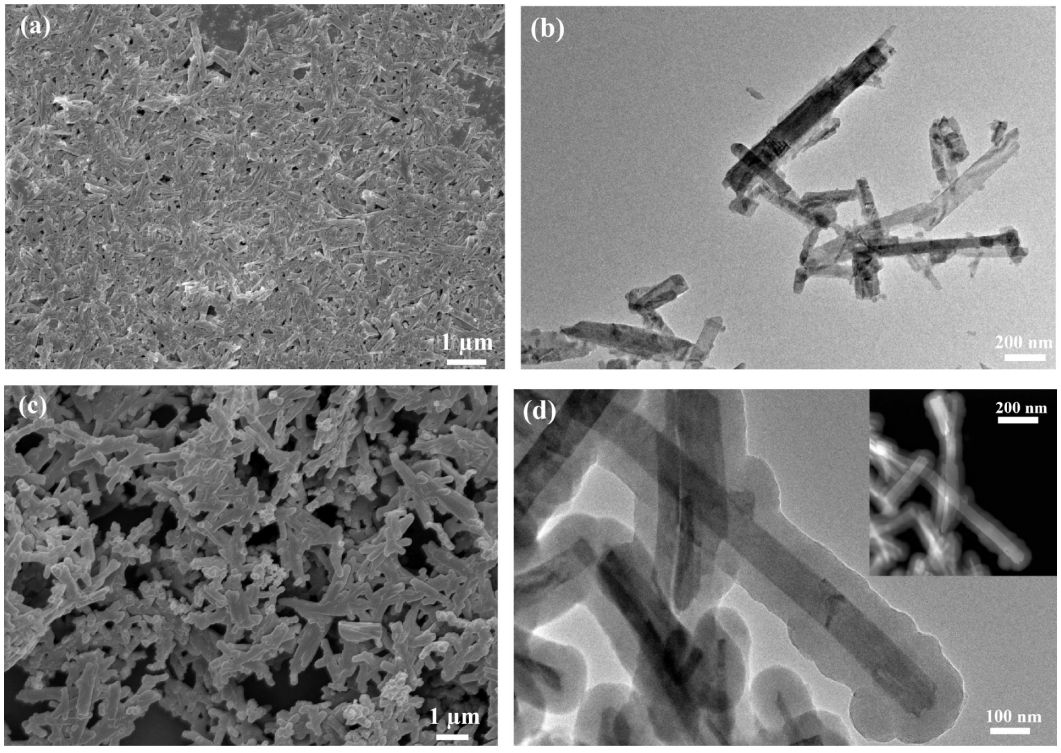

Figure 3. (a) FESEM and (b) TEM images of the pristine MoO_3 nanobelts and (c) FESEM and (d) TEM images of the MoO_3/PPy nanocomposite. The inset is the dark-field TEM image.

dx.doi.org/10.1021/am404724u | ACS Appl. Mater. Interfaces 2014, 6, 1125−1130

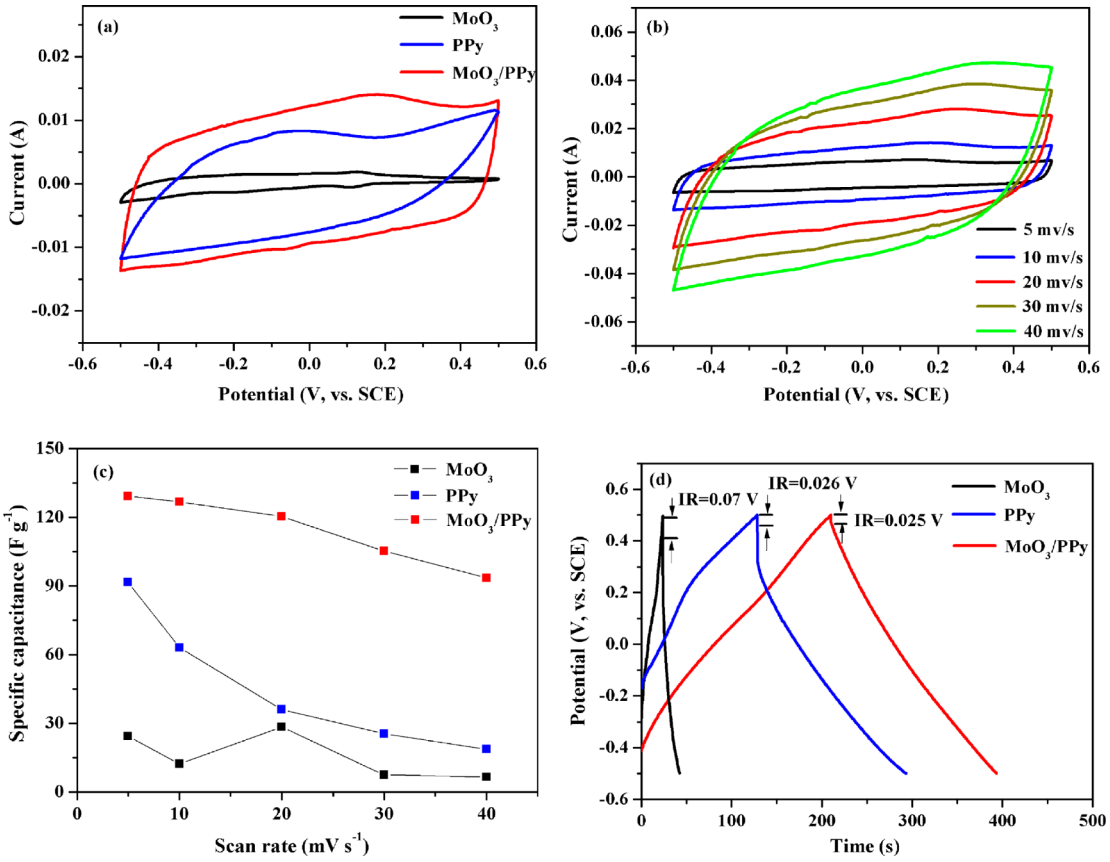

Figure 4. (a) CV curves of MoO_3, pure PPy, and MoO_3/PPy electrodes at a scan rate of 10 mV s^{-1}. (b) CV curves of the MoO_3/PPy nanocomposite at different scan rates. (c) Specific capacitances of MoO_3, pure PPy, and MoO_3/PPy electrodes at different scan rates. (d) Galvanostatic charge–discharge curves of MoO_3, pure PPy, and MoO_3/PPy electrodes at a current density of 0.67 A g^{-1}.

peaks, indicating a typical electrical double-layer capacitance feature with fast charging–discharging processes. Additionally, the shapes of these CV curves do not significantly change as the scan rate is increased from 5 to 40 mV s^{-1}, revealing the ideal capacitive behavior and good charge collection as well as the facilitated diffusion of Na^+ in the MoO_3/PPy nanocomposite electrode.[39] Moreover, as the scan rate decreased from 40 to 5 mV s^{-1}, the specific capacitances (C_s) of the MoO_3/PPy hybrid were enhanced from 93 to 129 F g^{-1}, which were calculated from the CV curves according to the following equation

$$C_s = \frac{\int I \, dV}{vm\Delta V} \quad (1)$$

where I (A) is the response current, v (V s^{-1}) is the scan rate, ΔV (V) is the potential window, and m (g) is the mass of active electrode material. According to eq 1, the maximum specific capacitance of 129 F g^{-1} observed in this measurement range is 5-fold higher than that of the pristine MoO_3 (24 F g^{-1}) and is also higher than the pure PPy (91 F g^{-1}; shown in Figure 4c). Considering that the capacitive performance strongly depends upon the electrical conductivity of the electrode, the low capacitance possessed by the bare MoO_3 nanobelts may be due to its poor internal conductivity. This conclusion can also be supported by the values of the IR drops in the galvanostatic charge–discharge curves of MoO_3 and the MoO_3/PPy hybrid at a current density of 0.67 A g^{-1}. Figure 4d shows that the IR drops are 0.07 and 0.025 V for the MoO_3 and MoO_3/PPy electrodes, respectively, indicating that the introducing of the PPy sheath in the MoO_3 nanobelts can greatly reduce the internal resistance, thus improving the transport and collection of electrons.

To obtain more information on the capacitive performance of the MoO_3/PPy nanocomposite, the galvanostatic charge–discharge test was selected for the successive measurement. Figure 5a gives the galvanostatic charge–discharge curves of MoO_3/PPy hybrid examined in 1 M Na_2SO_4 electrolyte at different current densities. The specific capacitances of the electrode can be calculated from the galvanostatic charge–discharge curves using the following equation

$$C_m = \frac{It}{m\Delta V} \quad (2)$$

where C_m (F g^{-1}) is the specific capacitance, I (A) is the discharge current, t (s) is the discharge time, ΔV (V) is the potential window, and m (g) is the mass of the active material. According to eq 2, the specific capacitances of the MoO_3/PPy hybrid are 123, 120, 109, and 104 F g^{-1} at 0.27, 0.67, 1.33, and 2.67 A g^{-1}, respectively (Figure 5b). At low current densities, the inner active sites or the pores of the electrode can be fully accessed and diffused with cations; hence, high specific capacitance values are achieved. According to the above results, the capacitance of the MoO_3/PPy hybrid electrode is obviously higher than the reported values.[13−15,30]

EIS measurements were performed to evaluate further the electrochemical performance of pristine MoO_3 and the MoO_3/PPy nanocomposite. Typical impedance plots for these two electrodes are displayed in Figure 5c. Both of the Nyquist plots are composed of a semicircle in the high-frequency range and a

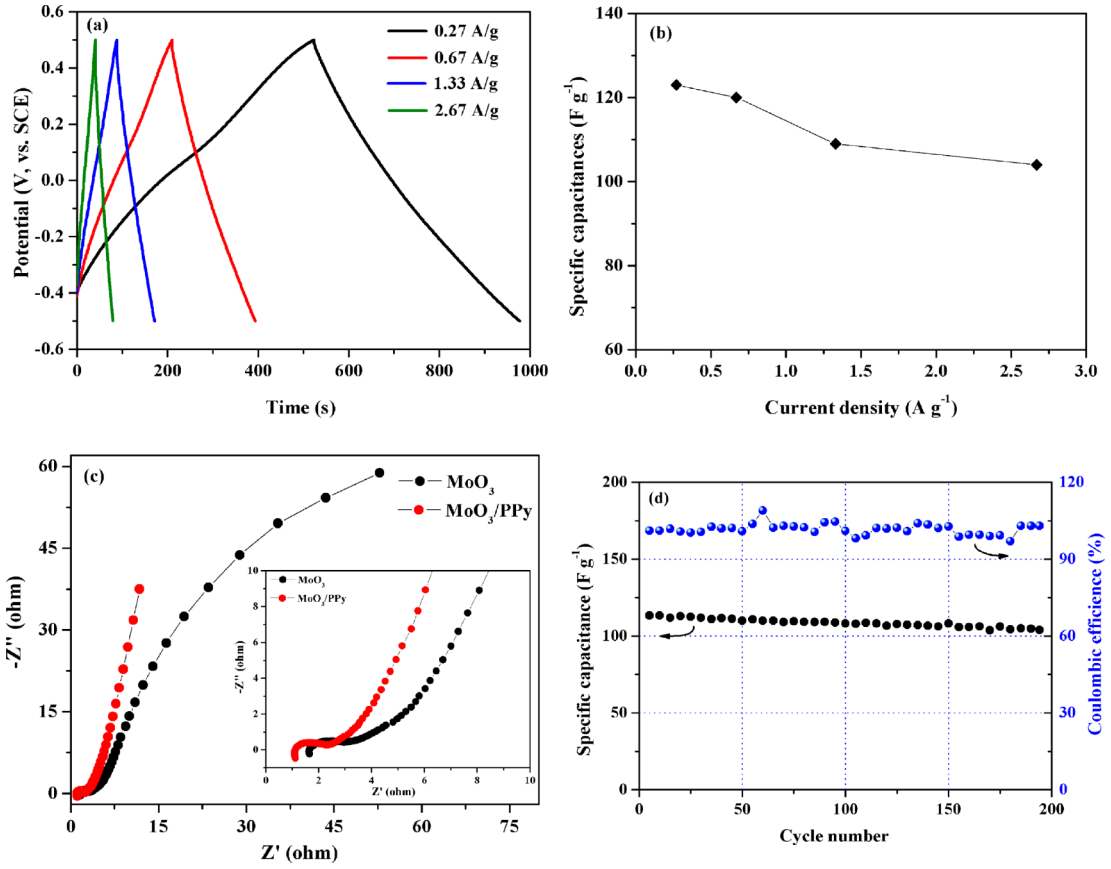

Figure 5. (a) Galvanostatic charge−discharge curves and (b) specific capacitances of the MoO_3/PPy nanocomposite at different current densities. (c) Nyquist plots of MoO_3 and MoO_3/PPy electrodes in 1 M Na_2SO_4 (the inset shows an enlarged scale). (d) Cycling stability and the Coulombic efficiency of the MoO_3/PPy nanocomposite at a current density of 0.67 A g^{-1}.

straight line in the low-frequency range. The intersection point of the semicircle on the real axis at high frequency represents the equivalent series resistance (R_s) of the electrode, whereas the diameter of the semicircle corresponds to the charge-transfer resistance (R_{ct}) of the electrode and electrolyte interface.[40,41] Comparing the impedance plots of these two electrodes, it is apparent that the value of R_s for the MoO_3/PPy hybrid is 1.11 Ω, which is significantly lower than the value of 1.64 Ω for the pristine MoO_3 nanobelts, suggesting that the MoO_3/PPy nanocomposite has very low internal resistance with good ion response in the high-frequency range. However, the almost vertical line in the low-frequency range is related to the diffusive resistance of the electrolyte into the interior of the electrode and the ion diffusion into the electrode, implying the ideally capacitive behavior of the MoO_3/PPy nanocomposite electrode.

The cycling stability is also an important factor to estimate the electrochemical behavior of the MoO_3/PPy electrode. In this study, the cycling performance was investigated by a galvanostatic charge−discharge test, which was carried out at a current density of 0.67 A g^{-1} in a potential range from −0.5 to 0.5 V (vs SCE). As shown in Figure 5d, a good cycling stability of the MoO_3/PPy nanocomposite can be achieved. Compared with the first cycle, the specific capacitance of this electrode still remains at 90% after 200 cycles, demonstrating that the MoO_3 nanobelts have excellent long-term cycling performance after being decorated by PPy conductive polymer. Furthermore, the Coulombic efficiency of the MoO_3/PPy hybrid electrode is around 100%, presenting a promising potential for their commercial application as a novel electrode material in supercapacitors.

4. CONCLUSIONS

A branchlike MoO_3/PPy nanocomposite with a high specific capacitance and long life-cycle was obtained by in situ oxidative polymerization of pyrrole monomer in the presence of a MoO_3 nanobelts suspension. The XRD characterization manifested that the coating of the PPy on the MoO_3 nanobelts surface did not impede the crystalline behavior of the pristine MoO_3. The electrochemical tests in 1 M Na_2SO_4 electrolyte revealed a good capacitive behavior for the MoO_3/PPy nanocomposite in a potential window from −0.5 to 0.5 V (vs SCE), implying that this novel nanocomposite has significant potential to be exploited further in supercapacitor devices.

AUTHOR INFORMATION

Corresponding Author

*E-mail: qiyx@licp.cas.cn.

Notes

The authors declare no competing financial interest.

ACKNOWLEDGMENTS

This work is supported by the Chinese Academy of Sciences and Technology Project (XBLZ-2011-013) and the Technologies R&D Program of Gansu Province (1104FKCA156).

REFERENCES

(1) Simon, P.; Gogotsi, Y. *Nat. Mater.* **2008**, *7*, 845−854.
(2) Stoller, M. D.; Park, S.; Zhu, Y.; An, J.; Ruoff, R. S. *Nano Lett.* **2008**, *8*, 3498−3502.
(3) Zhang, L. L.; Zhao, X. S. *Chem. Soc. Rev.* **2009**, *38*, 2520−2531.
(4) Huggins, R. A. *Solid State Ionics* **2000**, *134*, 179−195.
(5) Hu, C. C.; Chang, K. H.; Lin, M. C.; Wu, Y. T. *Nano Lett.* **2006**, *6*, 2690−2695.
(6) Huang, H. S.; Chang, K. H.; Suzuki, N.; Yamauchi, Y.; Hu, C. C.; Wu, K. C. W. *Small* **2013**, *9*, 2520−2526.
(7) Li, Z. P.; Mi, Y. J.; Liu, X. H.; Liu, S.; Yang, S. Y.; Wang, J. Q. *J. Mater. Chem.* **2011**, *21*, 14706−14711.
(8) Liao, M. X.; Liu, Y. F.; Hu, Z. H.; Yu, Q. *J. Alloys Compd.* **2013**, *562*, 106−110.
(9) Jena, A.; Munichandraiah, N.; Shivashankar, S. A. *J. Power Sources* **2013**, *237*, 156−166.
(10) Nasibi, M.; Golozar, M. A.; Rashed, G. *Mater. Chem. Phys.* **2013**, *139*, 12−16.
(11) Wang, F. X.; Xiao, S. Y.; Hou, Y. Y.; Hu, C. L.; Liu, L. L. *RSC Adv.* **2013**, *3*, 13059−13084.
(12) Tang, W.; Liu, L. L.; Zhu, Y. S.; Sun, H.; Wu, Y. P.; Zhu, K. *Energy Environ. Sci.* **2012**, *5*, 6909−6913.
(13) Mendoza-Sánchez, B.; Brousse, T.; Ramirez-Castro, C.; Nicolosi, V.; Grant, P. S. *Elecrochim. Acta* **2013**, *91*, 253−260.
(14) Sharkir, I.; Shahid, M.; Yang, H. W.; Kang, D. J. *Electrochim. Acta* **2010**, *56*, 376−380.
(15) Zhao, G. Y.; Zhang, N. Q.; Sun, K. N. *Mater. Res. Bull.* **2013**, *48*, 1328−1332.
(16) Brezesinski, T.; Wang, J.; Tolbert, S. H.; Dunn, B. *Nat. Mater.* **2010**, *9*, 146−151.
(17) Mai, L.; Hu, B.; Chen, W.; Qi, Y.; Lao, C.; Yang, R.; Dai, Y.; Wang, Z. L. *Adv. Mater.* **2007**, *19*, 3712−3716.
(18) Murugan, A. V.; Viswanath, A. K. *J. Appl. Phys.* **2006**, *100*, 074319−074325.
(19) Zheng, L.; Xu, Y.; Jin, D.; Xie, Y. *J. Mater. Chem.* **2010**, *20*, 7135−7143.
(20) Mahmood, Q.; Yun, H. J.; Kim, W. S.; Park, H. S. *J. Power Sources* **2013**, *235*, 187−192.
(21) Shakir, I.; Shahid, M.; Nadeem, M.; Kang, D. J. *Electrochim. Acta* **2012**, *72*, 134−137.
(22) Shakir, I.; Shahid, M.; Cherevko, S.; Chung, C. H.; Kang, D. J. *Electrochim. Acta* **2011**, *58*, 76−80.
(23) Takagi, S.; Makuta, S.; Veamatahau, A.; Otsuka, Y.; Tachibana, Y. *J. Mater. Chem.* **2012**, *22*, 22181−22189.
(24) Wong, H. P.; Dave, B. C.; Leroux, F.; Harreld, J.; Dunn, B.; Nazar, L. F. *J. Mater. Chem.* **1998**, *8*, 1019−1027.
(25) Biswas, S.; Drzal, L. T. *Chem. Mater.* **2010**, *22*, 5667−5671.
(26) Yan, Y.; Cheng, Q.; Wang, G.; Li, C. *J. Power Sources* **2011**, *196*, 7835−7840.
(27) Sharma, R. K.; Rastogi, A. C.; Desu, S. B. *Electrochim. Acta* **2008**, *53*, 7690−7695.
(28) Li, J.; Xie, H. Q.; Li, Y. *J. Power Sources* **2013**, *241*, 388−395.
(29) Dhibar, S.; Sahoo, S.; Das, C. K. *J. Appl. Polym. Sci.* **2013**, *130*, 554−562.
(30) Liu, Y.; Zhang, B. H.; Yang, Y. Q.; Chang, Z.; Wen, Z. B.; Wu, Y. P. *J. Mater. Chem. A* **2013**, *1*, 13582−13587.
(31) Oswald, H. R.; Gunter, J. R.; Dubler, E. *J. Solid State Chem.* **1975**, *13*, 330−338.
(32) Nagasawa, T.; Kobayashi, K. *J. Appl. Phys.* **1970**, *41*, 4276−4284.
(33) Subba, R. C. V.; Walker, J. E. H.; Chen, W.; Sunil, M. *J. Power Sources* **2008**, *183*, 330−333.
(34) Zakharova, G. S.; Täschner, C.; Volkov, V. L.; Hellmann, I.; Klingeler, R.; Leonhardt, A.; Büchneret, B. *Solid State Sci.* **2007**, *9*, 1028−1032.
(35) Kostic, R.; Rakovic, D.; Stepanyan, S. A.; Davidova, I. E.; Gribov, L. A. *J. Chem. Phys.* **1995**, *102*, 3104−3109.
(36) Acqua, L. D.; Tonin, C.; Peila, R.; Ferrero, F.; Catellani, M. *Synth. Met.* **2004**, *146*, 213−221.
(37) Blinova, N. V.; Stejskal, J.; Trchova, M.; Prokes, J.; Omastova, M. *Eur. Polym. J.* **2007**, *43*, 2331−2341.
(38) Yao, W.; Zhou, H.; Lu, Y. *J. Power Sources* **2013**, *241*, 359−366.
(39) Li, J.; Yang, Q. M.; Zhitomirsky, I. *J. Power Sources* **2008**, *185*, 1569−1574.
(40) Kim, C.; Ngoc, B. T. N.; Yang, K. S.; Kojima, M.; Kim, Y. A.; Kim, Y. J.; Endo, M.; Yang, S. C. *Adv. Mater.* **2007**, *19*, 2341−2346.
(41) Chen, S.; Zhu, J. W.; Wang, X. *J. Phys. Chem. C* **2010**, *114*, 11829−11834.